APPLICATIONS OF VORTEX-LATTICE THEORY TO PRELIMINARY AERODYNAMIC DESIGN

John W. Paulson, Jr.
NASA Langley Research Center

SUMMARY

This paper presents some applications of the vortex-lattice theory to the preliminary aerodynamic design and analysis of subsonic aircraft. These methods include the Rockwell-Tulinius vortex-lattice theory for estimating aerodynamic characteristics, a Trefftz plane optimization procedure for determining the span loads for minimum induced drag, and a modification of the Trefftz plane procedure to estimate the induced drag for specified span loads. The first two methods are used to aerodynamically design aircraft planforms, twists, and cambers, and the latter method is used to estimate the drag for components such as flaps and control surfaces.

Results from the theories for predicting lift and pitching moment, drag due to lift, and the drag of control surfaces are compared with experimental data. The data were obtained on a general aviation model with flaps and a close-coupled canard-wing model.

INTRODUCTION

In the preliminary stages of aircraft design, it is necessary that the designer have valid estimates of aircraft aerodynamics, particularly lift, drag, and pitching moments. Lift and pitching moment are required to size the planforms (wing, tail, and canard) and locate them with respect to a moment center, usually a desired aircraft center of gravity, for trimmed lift requirements and stability margins. Skin friction, form, and induced drags must be estimated and minimized for best performance. Many theoretical methods involving various levels of complexity have been developed which estimate these characteristics to varying degrees of accuracy. The preliminary designer, however, wants methods that are fast, reasonably accurate, and easy to use so that changes in aircraft configuration can be easily assessed. Once the overall configuration geometry is defined, he may wish to use some of the more highly sophisticated methods to refine his estimates before beginning experimental verification of the design. This paper will address applications of easy-to-use methods appropriate at the preliminary design stage; these methods include the Rockwell-Tulinius vortex-lattice theory for estimating aerodynamic characteristics, a Trefftz plane optimization procedure for determining the span loads for minimum induced drag, and a modification of the Trefftz plane procedure to estimate the induced drag for specified span loads.

SYMBOLS

A	aspect ratio, b^2/S
b	span
C_D	drag coefficient
$C_{D,i}$	induced drag coefficient
$C_{D,o}$	minimum drag coefficient
C_L	lift coefficient
C_{L_α}	lift-curve slope
C_m	pitching-moment coefficient
C_N	normal-force coefficient
c	chord
c_{avg}	average chord
$\bar{c}$	mean aerodynamic chord
c_l	section lift coefficient
c_n	section normal-force coefficient
E_v	y-component of influence function for pair of trailing vortex legs
E_w	z-component of influence function for pair of trailing vortex legs
e	induced-drag efficiency parameter, $C_L^2/C_{D,i}\pi A$
h	vertical separation between canard and wing
N_y	y-component of normal unit vector
N_z	z-component of normal unit vector
q	dynamic pressure
S	wing area
ΔS	incremental section width (from ref. 1)
T_y	tangent unit vector spanwise component

T_z tangent unit vector vertical component

V_∞ free-stream velocity

w downwash velocity

X,Y,Z axis system

x,y distance along X- and Y-axes

x_{mc} moment-center location

α angle of attack

Γ section circulation

δ_f flap deflection

η fraction of semispan, $y/b/2$

ρ density

Subscripts:

cp center of pressure

d design

j,k indices

max maximum

DISCUSSION

Prediction of Lift and Pitching Moment

The Rockwell-Tulinius unified vortex-lattice theory (refs. 1 and 2) can be used to predict static and rotary stability derivatives for configurations with multiple lifting surfaces of arbitrary shape. It can also compute the section and total configuration forces and moments for arbitrary planform geometries with twist and camber. This method, as programed, is fast, easy to use, and fairly accurate.

The agreement between this theory and experimental data for the lift of a simplified general aviation model is shown in figure 1. The model has a straight untapered wing using the NASA GA(W)-1 airfoil section (refs. 3 and 4) and had 2^o of twist (washout) from the root to the tip. The model body was a flat-sided ellipse. For the theoretical calculations, the fuselage was modeled as a flat plate and the wing as a camber line with twist. Agreement between the estimated C_L and the experimental C_L was quite good at low angles of attack prior to flow separation which occurred at $\alpha = 4^o$.

Also shown in figure 1 are the theoretical drag polars for 0-percent and 100-percent leading-edge suction as given by the equations

$$C_D = C_{D,o} + \frac{C_L^2}{\pi Ae}$$

for 100-percent leading-edge suction and

$$C_D = C_{D,o} + \frac{C_L^2}{C_{L_\alpha}}$$

for 0-percent leading-edge suction. The value for $C_{D,o}$ was obtained from the experimental data. These curves for 100-percent and 0-percent leading-edge suction represent the best and worst possible drag polars, respectively, for a given configuration. The leading-edge radius and/or camber design should produce data that are as close to the 100-percent suction polar as possible. Near-field analyses are required to minimize viscous and separated flow effects to approach the 100-percent suction polar. For this case, the data show that the design was close to the 100-percent suction polar up to $C_L = 1.2$.

Two-dimensional separation can be delayed and minimized for moderate angles of attack by proper planform shaping, camber design, and leading-edge-radius selection. However, at large angles of attack, the viscous form drag must be reduced by taking advantage of interfering flow fields of adjacent surfaces, vortex flows, or induced propulsion effects. Examples of applications of this approach for reducing viscous form drag due to lift are shown later in this paper.

Figure 2 is a sketch of a close-coupled canard model tested in the Langley V/STOL tunnel to investigate the effects of propulsion on stability at high angles of attack. A similar unpowered model was tested in the Langley high-speed 7- by 10-foot tunnel by Blair B. Gloss (ref. 5) to determine the effect of vortex lift on performance, especially $C_{L,max}$. The wings and canards of both models had symmetrical circular arc airfoil sections. Also, strakes were utilized in both tests to produce vortex lift at the higher angles of attack. The agreement between theory and data of Gloss (fig. 3) is good over the linear range of the data for the wing and the wing-canard configurations. The method does not predict the additional vortex lift and resulting pitching moment when the strake is present.

This method was used to establish a moment center for a wing-canard model to give a stability margin at low C_L of -5 percent $\left(\partial C_m/\partial C_L = 0.05\right)$ prior to testing in the V/STOL tunnel. The data, shown in figure 4, indicate a value of $\partial C_m/\partial C_L$ of about 0.06 to 0.05 at low C_L, which agrees well with the predi ted value.

Prediction of Minimum Induced Drag

Once the planforms of a configuration have been sized and located to meet lift and stability requirements, it is necessary to compute the optimum span loads for minimum induced drag for the interfering planforms. The expression for the induced drag was developed by using an equivalent lifting-line Trefftz plane approach of reference 1 and is illustrated by the following sketch and equation:

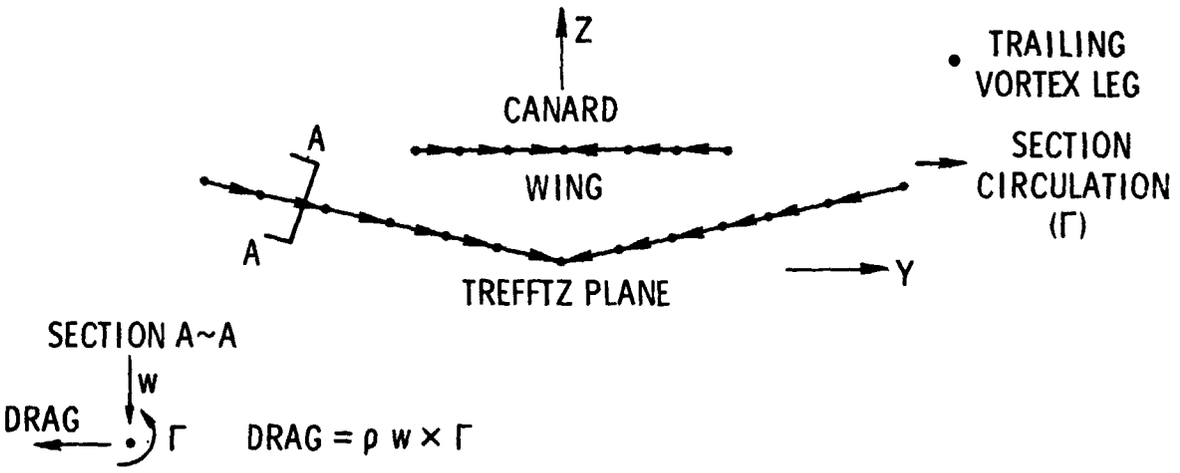

$$C_{D,i} = \frac{A}{2\pi b^2} \sum_{j=1}^{n} \sum_{k=1}^{n} \left(\frac{\Gamma}{V_\infty}\right)_j \left(\frac{\Gamma}{V_\infty}\right)_k \left[\left(E_{v,jk} T_{y,k} + E_{w,jk} N_{y,k}\right) T_{z,j} - \left(E_{v,jk} T_{z,k} + E_{w,jk} N_{z,k}\right) T_{y,j}\right] \Delta S_j$$

By utilizing the method of Lagrangian multipliers with the induced-drag equation, the span loads for minimum $C_{D,i}$ may be calculated while constraining C_L and C_m to desired values. This procedure was programed by Tulinius and Gloss, and the results are given in reference 2. The input for this program consists of the basic planform geometry, as in the Rockwell-Tulinius method, along with the desired $(x/c)_{cp}$ distribution. The $(x/c)_{cp}$ distribution is required to locate the chordwise position of the net span load for constraining the pitching moment and is generally selected from a desired two-dimensional section loading.

The method was applied to the close-coupled wing-canard model of Gloss and the results with and without constraints on C_m are presented in figure 5. The variation of the induced-drag efficiency parameter e is a function of wing-canard span ratio b_{canard}/b, wing-canard separation h/b, and wing-canard

lift ratio. The left side of figure 5 gives estimates of e when C_L is constrained and C_m is unconstrained. It can be seen that the estimated values of e increase as h/b and b_{canard}/b increase and are equal to or greater than 1.0. The right side of figure 5 gives estimates of e when both C_L and C_m are constrained to produce a trimmed configuration. It can be seen that the extra constraint lowers the values of e; however, e can still be greater than 1.0 if an upload on the canard is required for trim. When a canard or empennage download is required for trim, e is equal to or less than 1. In this figure, the location of the moment center was completely arbitrary and was chosen simply to give uploads and downloads on the canard.

A detailed study of the effect of moment-center location on e was performed for one configuration $\left(h/b = 0.09,\ b_{canard}/b = 0.68\right)$ and is presented in figure 6. It can be seen that e is a maximum at a moment-center location of about 10 percent $\bar{c}$ due to the nearly elliptic span loads present for this case. As the moment center is moved away from 10 percent $\bar{c}$, the loads required on the wing and canard for trim become more nonelliptic and e decreases accordingly.

It should be noted that the wing and canard must be twisted and cambered to produce the span loads required to approach the minimum $C_{D,i}$. The data of Gloss (ref. 5) were obtained for both flat and cambered wings in the presence of a canard. The cambered wings were designed to lift coefficients of 0.35 and 0.70. These experimental data are compared with the theoretical minimum value of $\dfrac{C_D - C_{D,o}}{C_L^2}$ in figure 7. The uncambered wing alone does not approach the theoretical minimum at low C_L because the sharp leading edge does not carry any leading-edge thrust. This wing departs drastically from the minimum at higher C_L because of the flow separation from the sharp leading edge. The downwash and vortex from the canard and strake retard the two-dimensional type of separation on the wing and the data show large improvements over the wing alone at higher C_L. However, the flat wing-canard-strake combination still does not approach the theoretical minimum because of the zero leading-edge thrust associated with the sharp leading edge. The cambered wings for the wing-canard configuration do approach the theoretical minimum at the design C_L because the cambered airfoil carries thrust on the camber line and the leading edge is drooped into the local flow direction to reduce the leading-edge flow separation.

Prediction of Induced Drag Due to Control Deflections

In addition to using the theory to aerodynamically design a configuration to meet the primary mission requirements, it is also useful in examining the effects of deflecting control surfaces and high-lift devices on the induced drag. A modification was made by Paulson and Thomas to the induced drag mini-

mization program to calculate the induced drag for specified span loads. The input span loads may be obtained either theoretically or experimentally. An example of the variation in span load due to two different types of flaps is shown in figure 8. This analysis was done on the general aviation model shown in figure 1 without the fuselage. The span loads were calculated by using the Rockwell-Tulinius method for the plain wing and for the wing with either slotted flaps or Fowler flaps deflected. Figure 9 shows the experimental drag polars for the three configurations. At $C_L = 1.0$, the calculated differences in induced drag between the plain wing and the wing with slotted flaps or Fowler flaps were 0.0010 and 0.0126, respectively. (See table 1.) The corresponding differences in the experimental data were 0.0012 and 0.0165, respectively. The additional skin-friction drag for the deflected Fowler flap (ref. 6) was estimated to be 0.0024. When this is combined with the computed induced drag, a total theoretical increment in drag of 0.0150 is obtained for the Fowler flap. This agrees well with the experimentally measured increment of 0.0165.

CONCLUDING REMARKS

Three applications of theoretical methods for preliminary aerodynamic design have been discussed. These methods are used to estimate wing and empennage geometries and locations to meet performance and stability requirements, to estimate span loads for minimum trimmed induced drag, and to analyze the effects of control surface deflection on induced drag. The theories are, in general, easy to use, fast, and the agreement with experimental data shows that they give accurate results. These methods are being used to design complex multiple lifting-surface models for experimental investigations in the Langley V/STOL tunnel.

REFERENCES

1. Tulinius, J.; Clever, W.; Niemann, A.; Dunn, K.; and Gaither, B.: Theoretical Prediction of Airplane Stability Derivatives at Subcritical Speeds. NASA CR-132681, 1975.

2. Tulinius, Jan R.; and Margason, Richard J.: Aircraft Aerodynamic Design and Evaluation Methods. AIAA Paper 76-15, Jan. 1976.

3. McGhee, Robert J.; and Beasley, William D.: Low-Speed Aerodynamic Characteristics of a 17-Percent-Thick Airfoil Section Designed for General Aviation Applications. NASA TN D-7428, 1973.

4. Paulson, John W., Jr.: Wind-Tunnel Tests of a Conventional Flap and Aileron and a Fowler Flap and Slot-Lip Aileron for an Advanced General Aviation Wing. SAE Paper 750501, Apr. 1975.

5. Gloss, Blair B.: Effect of Wing Planform and Canard Location and Geometry on the Longitudinal Aerodynamic Characteristics of a Close-Coupled Canard Wing Model at Subsonic Speeds. NASA TN D-7910, 1975.

6. Peterson, John B., Jr.: A Comparison of Experimental and Theoretical Results for the Compressible Turbulent-Boundary-Layer Skin Friction With Zero Pressure Gradient. NASA TN D-1795, 1963.

TABLE 1.- ESTIMATION OF DRAG INCREMENT DUE TO FLAPS FOR GENERAL AVIATION MODEL

$$\left[\Delta C_{D,i} + \Delta C_{D,\text{skin friction}} = \Delta C_{D,\text{estimated}}\right]$$

	C_L	C_D	$\Delta C_{D,i}$	$\Delta C_{D,\text{skin friction}}$	$\Delta C_{D,\text{estimated}}$	$\Delta C_{D,\text{exp}}$
Plain wing	1.0	0.0695	------	------	------	------
Slotted flap	1.0	.0707	0.0010	------	0.0010	0.0012
Fowler flap	1.0	.0860	.0126	0.0024	.0150	.0165

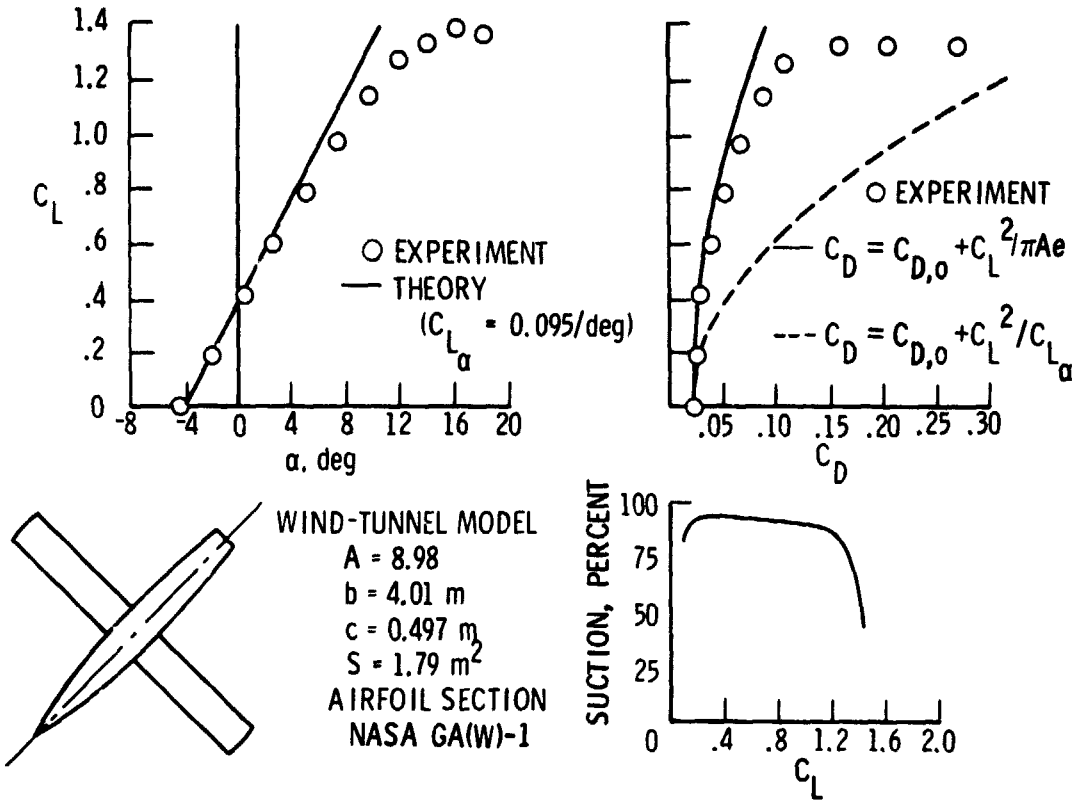

Figure 1.- Aerodynamic characteristics of general aviation model.

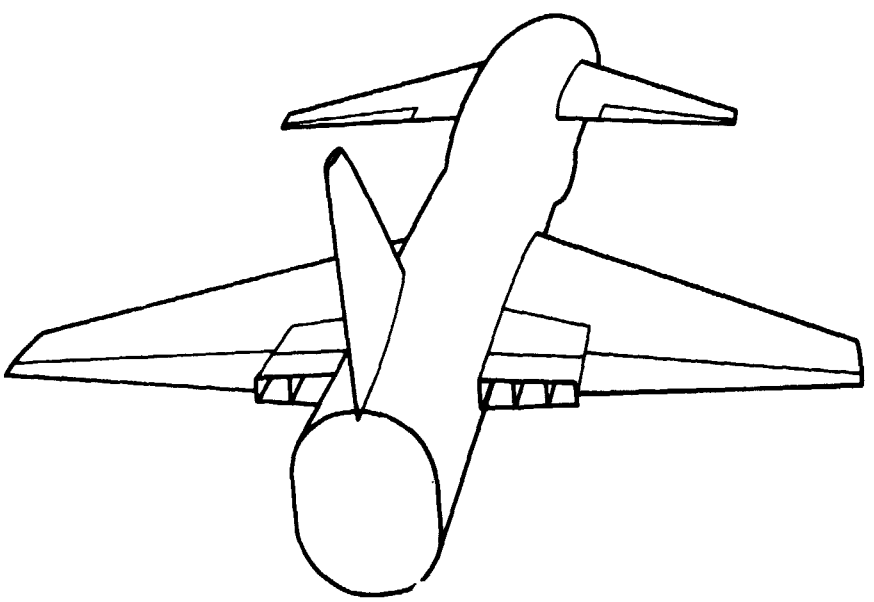

Figure 2.- Powered wing-canard research configuration.

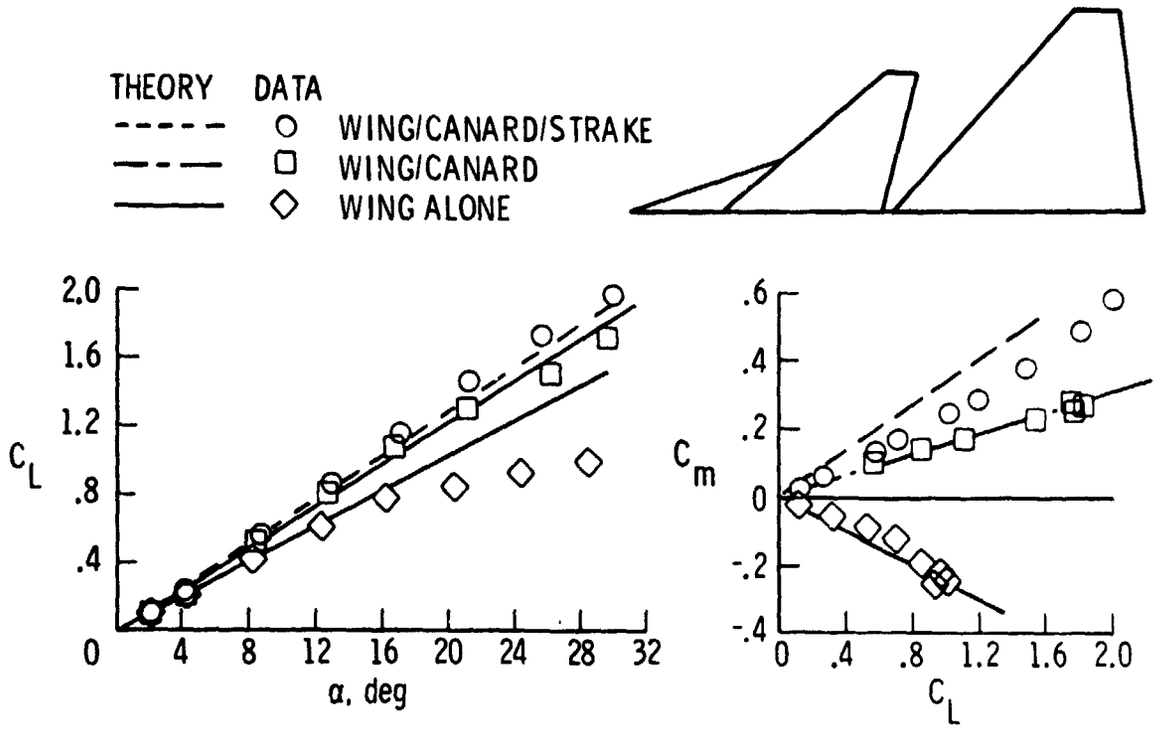

Figure 3,- Comparison between vortex-lattice theory and data. Theory from Rockwell-Tulinius vortex-lattice method; data from referebce 5.

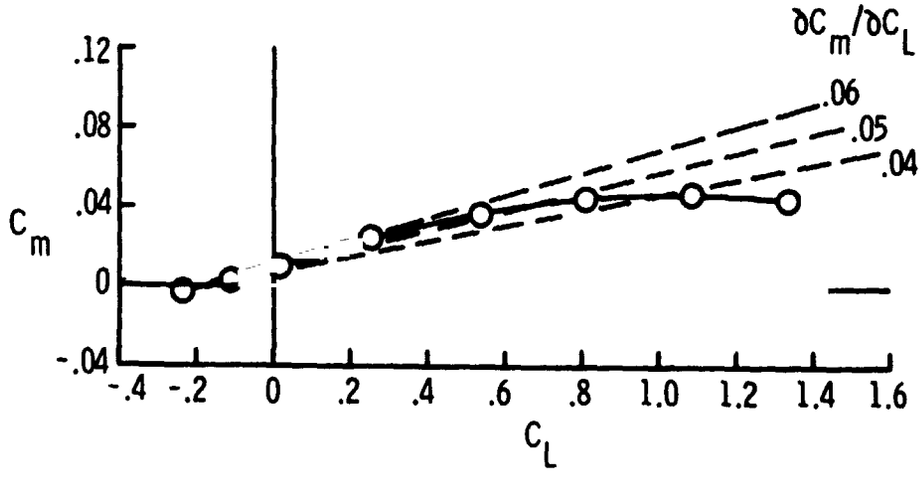

Figure 4.- Stability margin for model of figure 2.

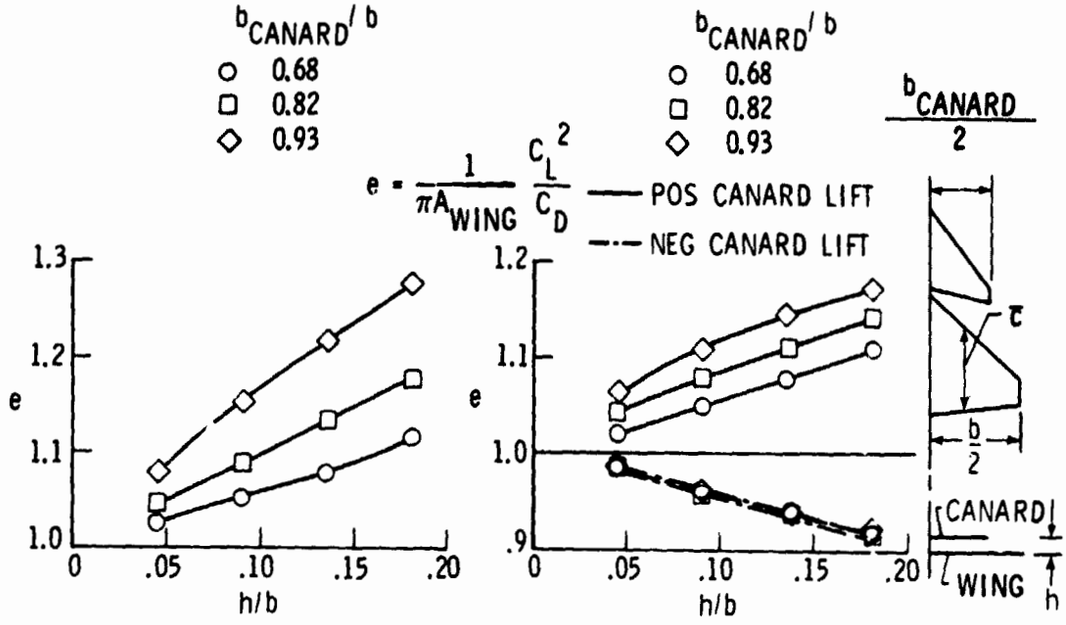

Figure 5.- Results from Trefftz plane vortex drag minimization theory. Equivalent lifting line approach.

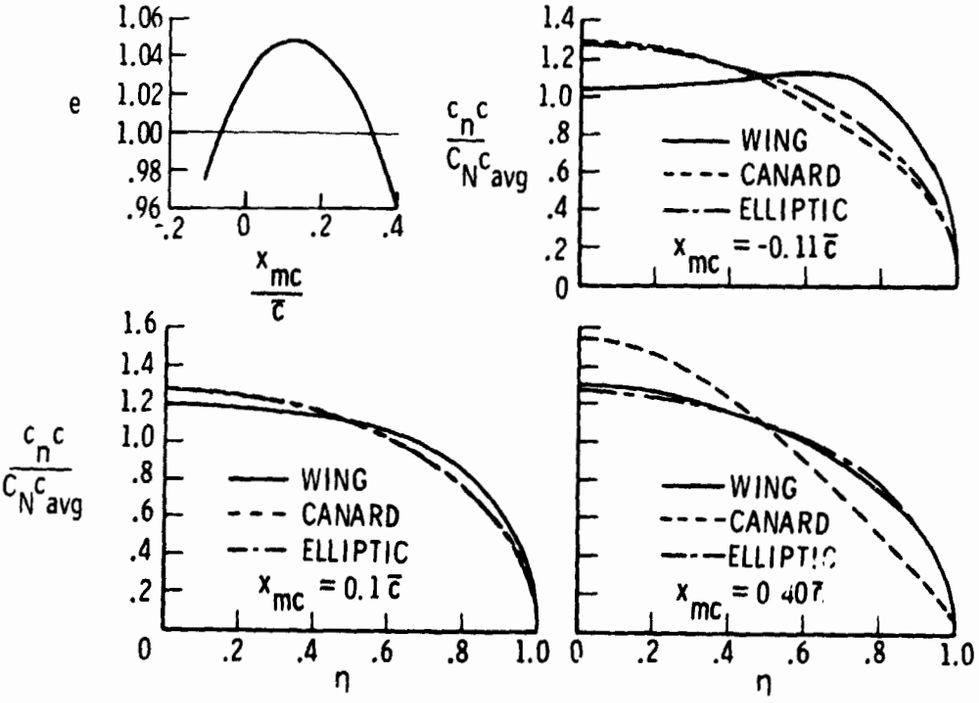

Figure 6.- Interference effects on optimum span load shape of the wing and canard.

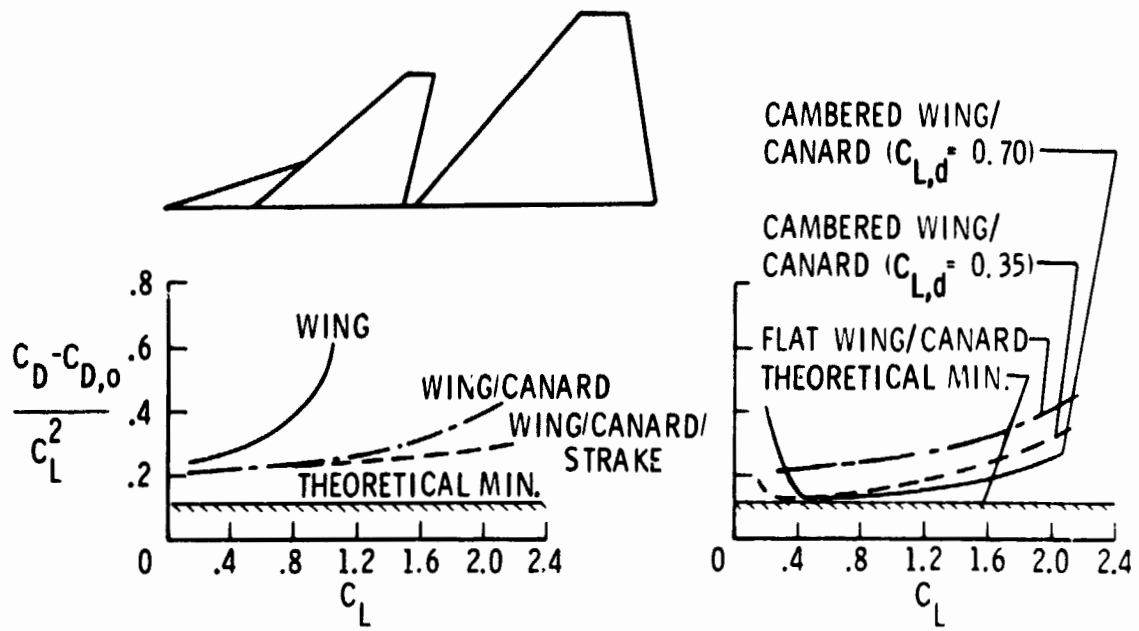

Figure 7.- Effects of canard, strake, and wing camber on drag due to lift.

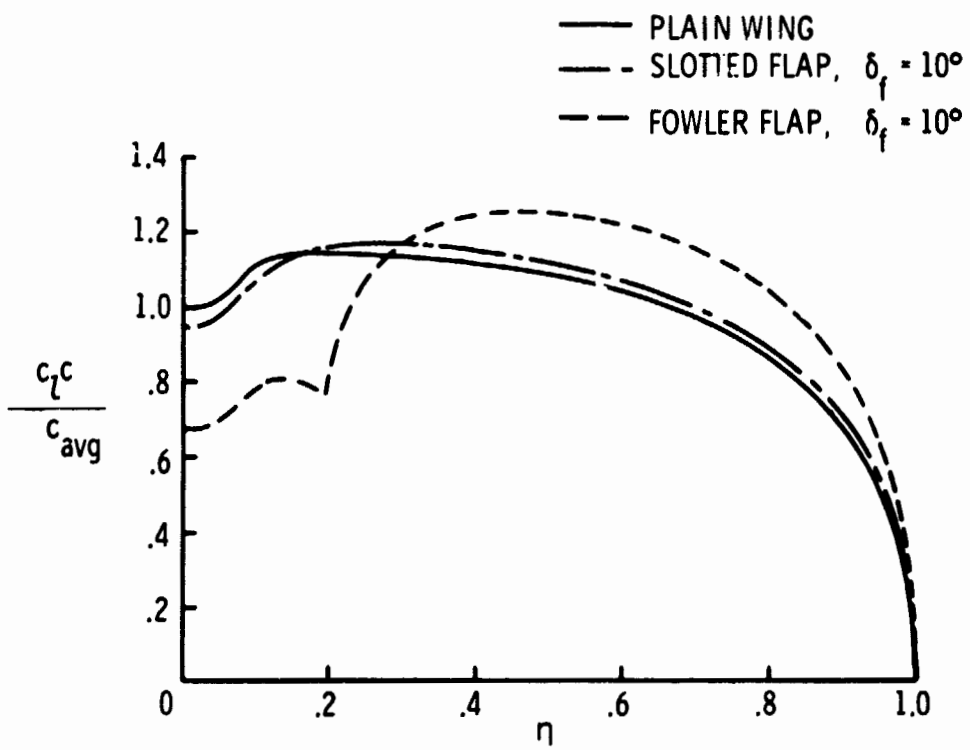

Figure 8.- Calculated span loads for general aviation model at C_L = 1.0.

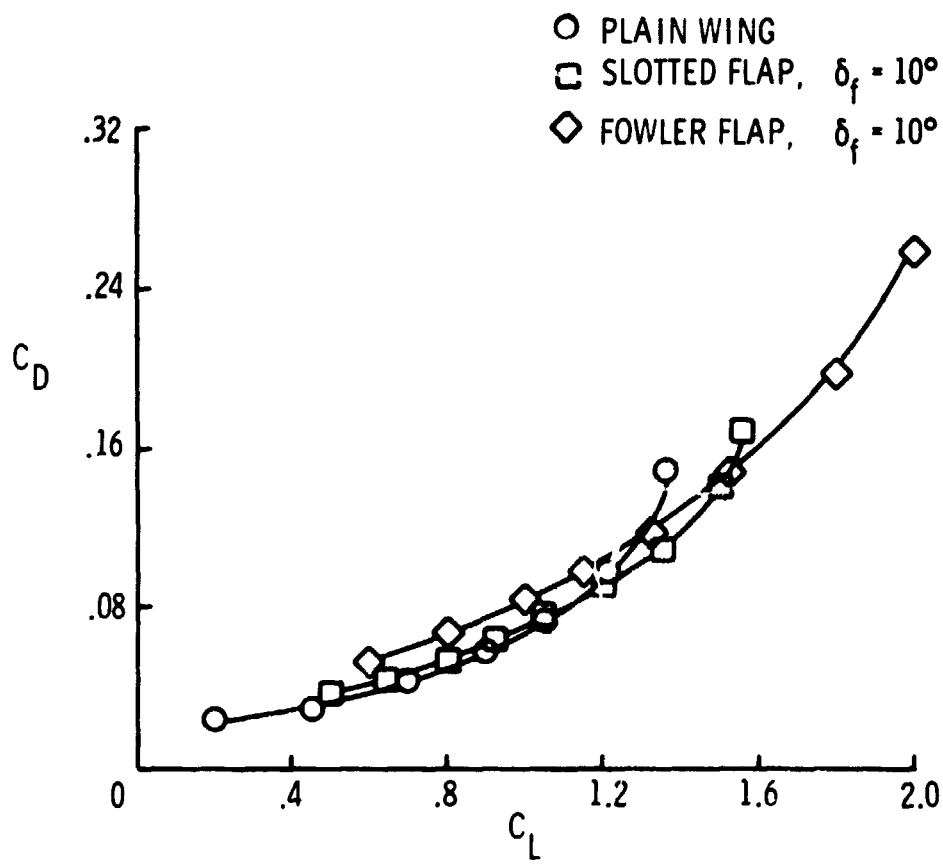

Figure 9.- Experimental drag polars for general aviation model.